doi: 10.5028/jatm.v9i4.831

Production and Characterization of Activated Carbon Fiber from Textile PAN Fiber

Miguel Angelo do Amaral Junior[1], Jorge Tadao Matsushima[1], Mirabel Cerqueira Rezende[2], Emerson Sarmento Gonçalves[3], Jossano Saldanha Marcuzzo[1], Maurício Ribeiro Baldan[1]

ABSTRACT: This paper presents the preparation and characterization of carbon fiber felt and activated carbon fiber felt from textile polyacrylonitrile fiber. Carbon fibers are usually related to aircraft manufacturing or high mechanical purposes. Activated carbon fibers are known as excellent adsorbent materials. Despite all advantages, carbon fiber and activated carbon fiber are expensive materials because of their raw material cost. On the other hand, in this study, carbon fiber felt and activated carbon fiber felt were produced from textile polyacrylonitrile fiber, which is cheaper than their precursor, polyacrylonitrile fiber, and can be converted into carbon fiber felt and activated material with high micropore content and surface area. This research describes the transformation of textile polyacrylonitrile fiber in its oxidized form. After that, the oxidized material was transformed in felt and, in the sequence, converted into carbon fiber felt and activated carbon felt. The carbon fiber felt and activated carbon fiber felt were characterized by X-ray photoelectron spectroscopy, Raman spectroscopy and scanning electron microscope. N_2 isotherms were performed to qualify the material obtained for further electrochemical applications. The main result was the conversion dynamics of textile polyacrilonitrile fiber into carbon fiber in felt form and activated carbon fiber in felt with high surface area and high micropores content.

KEYWORDS: Carbon fiber, Activated carbon fiber, Raman spectroscopy.

INTRODUCTION

Activated Carbon Fiber Felt (ACFF) has special characteristics when compared with common activated carbons (granular or powder). It can be transformed into fabric, woven or yarn forms which gives them self-sustainable characteristics. In addition, ACFF shows well-defined pore structures on its surface providing a high and fast adsorption capacity for specific components, such as for specific components with small molecular dimensions as ions, metals or organic. One of the most important characteristics, which makes ACFF a very special adsorbent material, is its pore size distribution (Suzuki 1994). In the ACFF case, a large amount of micropores can be found directly connected on their surface leading to a faster and less energetic adsorption mechanism, especially for gases (Cuña *et al.* 2014). ACFF is widely used in many applications such as air purification and water treatment, chemical (adsorption and desorption for organic compounds and solvents), military area such as protection garment and masks (Marsh and Reinoso 2006). The density of ACFF is considerably lower than the regular carbon fiber, making it ideal for applications requiring low weight. Despite all the advantages of Carbon Fiber Felt (CFF) and ACFF application, their use has been limited due to their relatively high cost.

The use of the textile type polyacrilonitrile (PAN) fiber to produce CFF and ACFF is a way to produce a material having an attractive surface area and some studies show this possibility (Carrott *et al.* 2001; Nabais *et al.* 2005; Marcuzzo *et al.* 2012). The use of standard textile fiber as raw material to make CFF

1.Instituto Nacional de Pesquisas Espaciais – Coordenação de Laboratórios Associados – Laboratório Associado de Sensores e Materiais – São José dos Campos/SP – Brazil. **2.**Universidade Federal de São Paulo – Instituto de Ciência e Tecnologia – Curso de Engenharia de Materiais – São José dos Campos/SP – Brazil. **3.**Departamento de Ciência e Tecnologia Aeroespacial – Instituto de Aeronáutica e Espaço – Divisão de Materiais – São José dos Campos/SP – Brazil.

Author for correspondence: Miguel Angelo do Amaral Junior | Instituto Nacional de Pesquisas Espaciais – Coordenação de Laboratórios Associados – Laboratório Associado de Sensores e Materiais | Avenida dos Astronautas, 1.758 – Jardim da Granja | CEP: 12.227-010 – São José dos Campos/SP – Brazil | Email: miguel.junior.mat@hotmail.com

Received: Nov. 03, 2016 | **Accepted:** Feb. 16, 2017

and ACFF is a way to make this material economically attractive (Yoon *et al.* 2004). Containing more than 95% of carbon, CFF and ACFF made from textile PAN have low electric resistance and they show potential application for catalytic process, especially when combined with metallic particles or in the form of films (Chung 2004; Pierozynski 2012). The CFF and ACFF can also be used as electrodes. The aim of this study is to present the production and characterization of CFF and ACFF made from a standard textile PAN.

MATERIALS AND METHODS

MATERIAL

The commercial 200 ktex tow of 5.0 dtex textile PAN fibers was thermal oxidized in a laboratory scale oven set by, aiming the production of flame resistant fibers. The oxidation process was performed in 2 steps, the first at 200 °C and the second at 300 °C. The total time process was 50 min for each step. After that, the oxidized PAN produced was used as a raw material to produce felt with 200 g/m^2 and about 3 mm thickness. The oxidized PAN fiber felt was carbonized, resulting into CFF. After that, the CFF was submitted to activation process to obtain the ACFF (Marcuzzo *et al.* 2012).

During the carbonization process, the oxidized PAN loses about 50% in mass and shrinks linearly about 10%. The shrinkage is an important parameter and must be controlled because an inadequate shrinkage result in poor mechanical characteristics and the fiber can not be handled. For this purpose, the oxidized PAN fiber felt sample was cut into pieces of about 0.7 × 0.25 m and placed in a special sample holder that can control the sample shrinkage in 2 dimensions.

The set was then introduced in an electrical furnace. Both ends of the furnace tube were closed by flanges, which allowed the insertion and the purge of processing gas to provide an atmosphere condition necessary for the carbonization and activation. The carbonization was performed in argon atmosphere at a final temperature of 1,000 °C at a heating rate of 30 °C/min. The process time at maximum temperature was set in 20 min to complete the carbonization process. After finishing the carbonization process, the furnace was turned off and maintained in Ar atmosphere. This condition of inert atmosphere was maintained until the room temperature inside the furnace reactor was reached.

The CFFs were carbonized at 900 °C, prior to activation, which was immediately accomplished at 1,000 °C, replacing the Ar gas by CO_2 gas, during 50 min. The activation time was previously defined by tests where the mechanical evaluation was done (Marcuzzo *et al.* 2012). The activation time of 50 min was fixed to guarantee the minimal mechanical condition to complete the carbonization process.

METHODS

The characterization was performed by gas adsorption aiming the measurements of surface area and pore size distribution function. The isotherm was performed by Beckman Coulter SA 3100 equipment. The Brunauer, Emmett, Teller (BET) method was applied to determine the total surface area and the pore size distribution was estimated by applying the Non-Local Density Function Theory (NLDFT) method over the adsorption isotherm, and the micropore volume was also estimated by the same method (Marsh and Reinoso 2006). The burn-off was estimated weighing the sample before and after the activation process.

The structural characterization of the CFF and ACFF were carried out by micro-Raman scattering spectroscopy (Renishaw Microscopy - 2000). Using the 514.5 nm line of an Ar ion laser taking the spectra at the range from ~ 800 to ~ 1,800 cm^{-1}. The optical microscope was used to excitation laser beam onto the sample and to collect the backscattered light. The diameter of the laser spot on the sample surface was 0.45 μm for the fully focused laser beam at 50X objective magnification. The instrument was calibrated using a pure diamond crystal. From the Raman spectroscopy, it was possible, quantitatively, to evaluate the change in the graphite organization through fitting by a combination of 4 Lorentzian bands (L, D_1, D_2, D_4) and a Gaussian band (D3) (Sadezky *et al.* 2005).

The morphological aspects of the CFF and ACFF were evaluated by scanning electron microscopy (SEM) using a JEOL JSM microscope. All the X-ray photoelectron spectroscopy (XPS) measurements were carried out with a Kratos Axis Ultra XPS spectrometer using a monochromatic Al-K_{alpha} (1,486.5 eV) X-ray radiation with power of 15 kV at 150 W. The emitted photoelectrons were detected using a hemispherical analyzer at 15 μm spatial resolution. The vacuum system was maintained at approximately 10^{-9} Torr during all the experiments. Survey scans were collected from 0 to 1,100 eV with a passing energy equal to 160 eV with step size of 1 eV to identify the elements present on the surface. Using the X-ray diffraction, it was possible to obtain information related to the crystalline structure. To carry out these measures, we used a PANalytical diffractometer serie X'PertPRO.

RESULTS AND DISCUSSION

SURFACE TEXTURE ANALYSIS

The aim of this topic is to show the characterization of CFF and ACFF. The carbonized fiber felt material, in theory, has about no significant surface area. The nitrogen isotherm technique was not able to show information about CFF surface area; consequently, it was considered smooth and without pores. On the other hand, for ACFF, the N_2 adsorption at 77 K isotherm showed significant information about surface texture. The isotherm is shown in Fig. 1 and is typically type I isotherm with no hysteresis and the saturation occurring at 0.2 relative working pressure and atmospheric pressure (P/P_0).

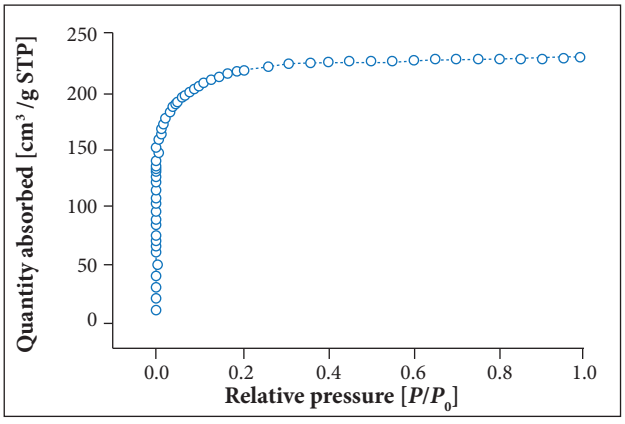

Figure 1. Nitrogen isotherm of ACFF at 77 K.

These results indicate that this activated material is predominantly populated with micropores. The pore size distribution curve is shown in Fig. 2, and it clearly shows that the maximum pore width presented is around 2 nm and the predominant pores are sized at around 1.2 nm. This technique does not give information about pores sized less than 1.0 nm, because of N_2 penetration limit. However, it can be clearly observed in this curve that the distribution in the region for a width less than 1 nm is ascendant in the direction of origin. This fact infers that pore volume and surface area of micropores may be bigger than those calculated by using these isotherms. The main ACFF characteristics are presented in Table 1.

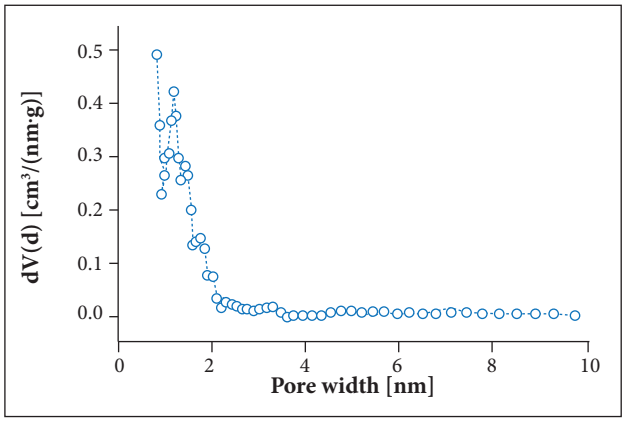

Figure 2. Pore size distribution curve of ACFF by NLDFT.

Table 1. Surface characteristics of ACFF.

Sample	Burn off (w%)	BET (m²/g)	$V_{micropore}$	V_{total}
ACFF	35	1,260	0.53	0.59

X-RAY PHOTOELECTRON SPECTROSCOPY DATA

XPS has proved a powerful method for the investigation of carbon surfaces (Kim and Park 2011; Ma *et al.* 2013). XPS surface characterization method combines surface sensitivity with the ability to quantitatively obtain both elemental and chemical state information. The surface chemistry of carbons is determined by the distribution and the nature of the surface functional groups. Many different functional groups can be identified on carbon surface. The information of all elements can be obtained from the survey scan spectrum of XPS. Vision software was used to calculate atomic concentrations. From survey spectra, atomic concentrations were calculated using peak areas of elemental lines.

X-Ray Photoelectron Spectroscopy Survey Spectra

Figure 3 shows the XPS survey spectra from which the elemental composition of the most external surface of the CFF

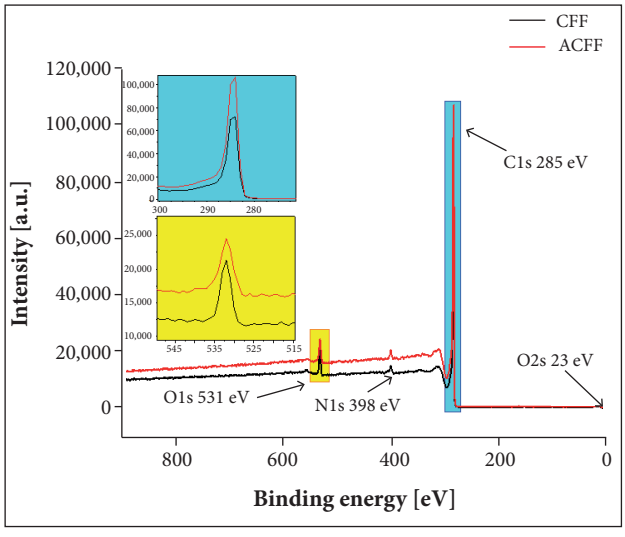

Figure 3. XPS survey spectra (a) CFF and (b) ACFF.

and ACFF samples was revealed. The spectra indicate that the major peaks in the spectra were due to the C 1s and O 1s, and a smaller N 1s peak is also discernible.

The contribution of the XPS technique in this work is the precise identification of the elements present on the surface of CFF and ACFF samples. The elemental composition (in %) on the CFF and ACFF samples were summarized in Table 2. XPS survey spectra showed the presence of less than 4.0% of oxygen on the surface of CFF and ACFF. The ACFF displayed O/C ratio of 2.42% while CFF showed higher O/C ratio of 4.05%. The same behavior was observed in the relative percentages of N/C atoms decreasing from 2.79 to 1.75% after the activation process.

Table 2. Elemental composition and N/C and O/C ratio for the CFF and ACFF samples.

Sample	C (%)	O (%)	N (%)	N/C	O/C
CFF	93.61	3.79	2.61	2.79	4.05
ACFF	96.00	2.32	1.68	1.75	2.42

The elemental composition and N/C as well as O/C ratio show a chemical surface change after the activation process. Besides, a slight increase in the amount of carbon was observed. The contribution of the XPS technique in this work is the precise identification of the elements present on the surface of CFF and ACFF samples. As expected, carbon, oxygen and nitrogen have been found on the surface of both fibers. In Fig. 3, it was observed that the carbon peak intensity is higher for ACFF. On the other hand, it may be observed a decrease in the oxygen amount after the activation process. In other words, the activation process contributed to the removal of the oxygen layer on the CFF, increasing the amount of carbon on the surface of ACFF.

RAMAN ANALYSIS

Raman spectroscopy is a technique widely used for analyzing carbon-based materials due to its sensitivity to different carbon structures, which produce distinctive Raman peaks for various forms of carbon. For example, the exact frequencies of the Raman bands of diamond, graphite, and amorphous forms of carbon depend on the crystallite size and stress present in the different carbon domains. The graphitic materials consist of a large number of peaks. However, the most intense broad bands are the *G* and *D*. In this paper, the *D* band is assigned as D_1. Raman spectra have been analyzed following Sadezky *et al.* (2005). Figure 4 shows the Raman spectra of the CFF and ACFF samples. The spectra consist of 2 major peaks attributed to D_1 and *G*. The *G* peak corresponds to the 1st-order Raman. The band frequency *G* (~ 1,584 cm^{-1}) is the E_{2g} 1st-order mode at the Brillouim zone center (gamma point). The *G* peak is due to the C-C bond stretching of all pairs of sp^2 atoms in both rings and chains. In particular, the G peak is the main Raman signature for sp^2 carbon. The spectra also exhibit additional first-order band characterized by a disorder that represents a zone-edge A_{1g} mode. Since the D_1 band is activated by defects, its intensity can be used to quantify disorders. Besides, it is used to characterize the microcrystallite size (L_a), which can be estimated from the ratio between D_1 and *G* bands by using the method of Tuinstra and Koenig (1970). Thomsen *et al.* (2004) were the first to explain the Raman spectra of the *D* mode using the concept of double resonances for a given laser energy and phonon branch. The origin and dispersion of the *D* band in carbon materials were also investigated by Matthews *et al.* (1999). To explain the physical basis, these authors discussed the 2-D electron and phonon dispersion curves for graphite and concluded that the electronic transition only occurs in the

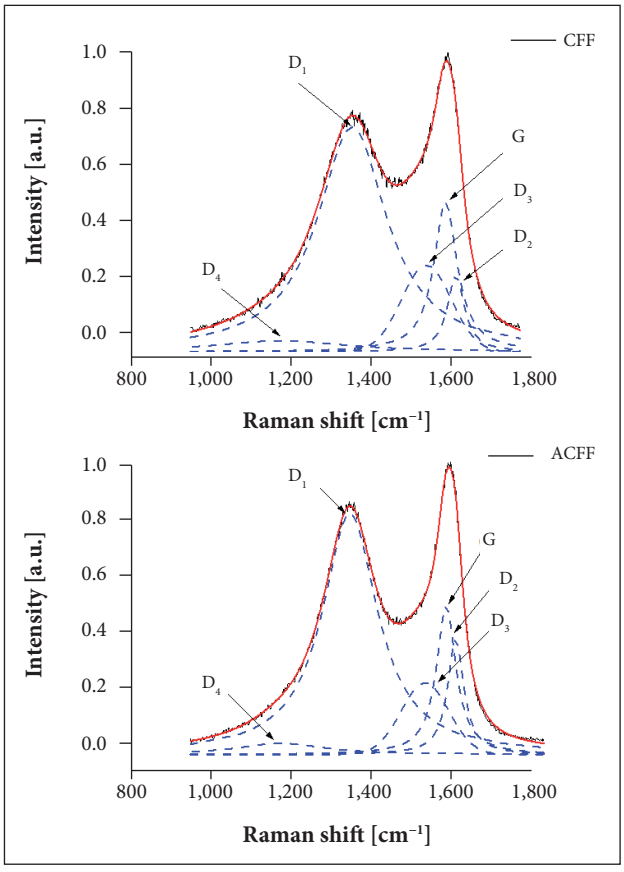

Figure 4. Raman spectra of the CFF and ACFF.

vicinity of the K point in the Brillouin zone. In the literature, it has been accepted that the relationship between band intensities is proportional to the degree of organization of carbonaceous materials. However, this relationship has been used in different forms as $(I_{D1}/I_G)_{A,H}$ or $(I_{D1}/(I_G + I_{D1}))_{A,H}$. The subscripts *A* and *H* indicate that the ratio is based on integrated intensities or peak heights, respectively. Beyssac *et al.* (2003) proposed to characterize the organization using $R_2 = (I_{D1}/(I_G + I_{D1} + I_{D2}))_{A,H}$. In this study, we tested the 3 different forms used in the literature. Besides, Lobo *et al.* (2005) considered the intensity values obtained from the integration of the *D* and *G* bands instead of using the ratio of the peak heights. In other words, the effect of line broadening is included in their calculation.

Special care should be taken to define a baseline to compare one spectrum to another. It is very important to point out that the decomposition is very sensitive to the choice of baseline. A linear baseline was chosen for both spectra to be the most appropriate. Raman spectra of the CFF and ACFF samples were submitted to deconvolution to separate *G* and D_1 peak in the first order by fitting as a sum of the Lorentzian-shaped *G*, D_1, D_2 and D_4 bands, as well as the Gaussian-shaped D_3 band. The reason for the D_3 band being Gaussian-shaped is because it presents better fit with the experimental data (Sadezky *et al.* 2005) and this study is also in agreement with this result. The fitting accounts the totality of the signal. It is noteworthy that both spectra *G* and *D* bands overlap each other to some extent. The overlapping is very important when we consider the integrated intensities. The spectra were recorded at different positions on the surface and looked very similar. The proportions in which the band participates are reported in Fig. 4 and the parameters used to calculus in Table 3. There is an appreciable difference in the absolute value of the 3 different forms to characterize carbonaceous materials. However, when we analyze each one individually, the ratio based on integrated intensities or peak heights did not present significant difference. By comparing the 3 different forms presented (Fig. 5), it is possible to verify that $I_{D1}/(I_G + I_{D1})_{A,H}$ and $I_{D1}/(I_G + I_{D1} + I_{D2})$ are more dispersive than I_{D1}/I_G. Several authors (Tuinstra and Koenig 1970; Thomsen *et al.* 2004; Matthews *et al.* 1999; Beyssac *et al.* 2003) discuss the *D* and *G* band intensity ratios (I_{D1}/I_G) and full width at half maximum for *G*-band (FWHM-*G*) and for *D*-band (FWHM-*D*) decrease with the increasing degree of crystalline. By considering the integrated intensities of *D* and *G*, our results reveal that (I_{D1}/I_G) for both CFF and ACFF are very close. However, according to Table 3, the FWHM-D_1 changes from 210.87 for CFF to 167.01 cm^{-1} for ACFF present a decrease of approximately 21%. Besides, the FWHM-*G* decreased after the activation processing by 17%. The decrease can be interpreted as some kind of transition related with the temperature during the activation process. Probably, it is related with the decrease in oxygen during the activation process as can be observed in XPS measurements. This indicates that defects were not introduced

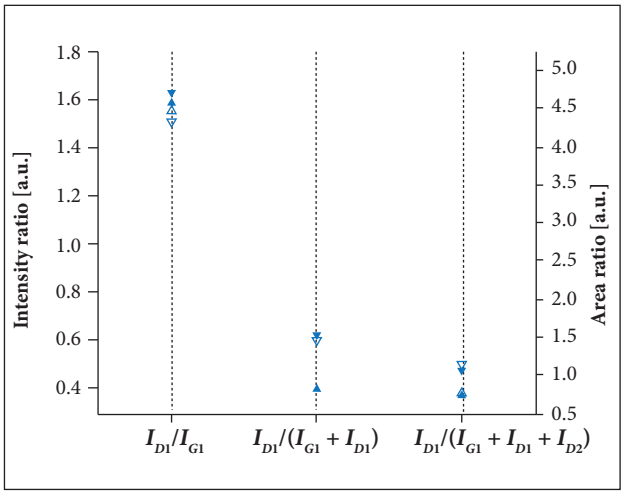

Figure 5. Calculation of the different ratio involving I_G, I_{D1} and I_{D2} bands.

Table 3. Fitting parameters of the *G*, D_1, D_2, D_3 and D_4 bands for the CFF and ACFF samples.

Band	Line shape	CFF - Sample			ACFF - Sample		
		Area	Center	FWHM	Area	Center	FWHM
D_4	Lorentz	25	1,173.71	401.34	16.29	1,173.14	257.66
D_1	Lorentz	266.70	1,351.36	210.87	225.04	1,344.24	167.01
D_3	Gaussian	48.27	1,536.53	146.32	37.88	1,530.21	139.14
G	Lorentz	59.44	1,584.32	71.09	48.91	1,582.81	59.01
D_2	Lorentz	22	1,610.46	51.38	31.43	1,606.48	49.01

during the process of activation. In fact, this indicates a small organization of the ACFF. Recently, Mallet-Ladeira *et al.* (2014) and Hu *et al.* (2015) reported different fitting procedures; the authors claim that their procedures are the most appropriate. There is a considerable controversy regarding fitting procedures. In this study, we consider that the most appropriated procedure for our results is to deconvolute the spectra utilizing multi-bands as reported in Sadezky *et al.* (2005). After analyzing the 3 different forms, we conclude that the variations of FWHM are no reflected in the (I_{D1}/I_G) form. On the other hand, the relation $I_{D1}/(I_G + I_{D1})_{A,H}$ and $I_{D1}/(I_G + I_{D1} + I_{D2})$ indicates that the structure of the CFF was changed after the activation process, which may be related to the production of surface defects after the removal of surface radicals from the sample.

X-RAY PHOTOELECTRON SPECTROSCOPY ANALYSIS

Figure 6 illustrates the XRD spectra for the CFF and ACFF samples. The diffratogram pattern of these samples exhibits 2 distinctive broad reflections in the θ angles located approximately at 25 and 44°. The peak broadening is an indicative of an amorphous structural aspect. The broad reflection in the 20 at 25° and 44° are associated with (002) and (001) diffraction line, respectively.

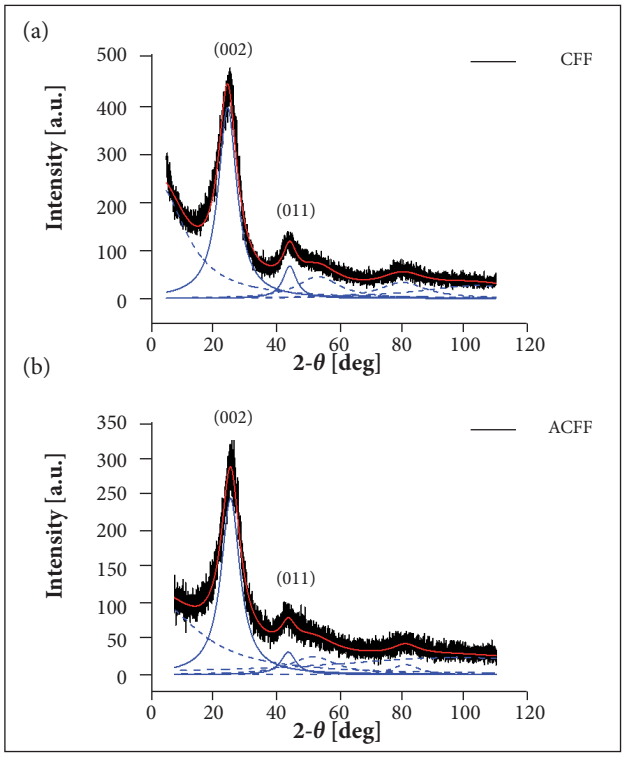

Figure 6. XRD spectra for (a) CFF and (b) ACFF samples.

From the X-ray diffraction (XRD) patterns of the CFF and ACFF, the lateral size (L_a) and stacking height (L_c) parameters were calculated using the Scherrer equation (Warren 1969) — Eqs.1 and 2, respectively. For calculation of L_a and L_c, we applied the Scherrer constant k_c equal to 0.9 for (002) diffraction line and k_a equal to 1.77 for (011) diffraction line, where λ (0.15 nm) is the wavelength of the X-ray used; β_{011} and β_{002} are full width at half maximum of the diffraction line (002) and (011). The results are summarized in Table 4.

$$Lc = \frac{k_c \lambda}{\beta_{002}\, cos\theta} \quad (1)$$

$$La = \frac{k_a \lambda}{\beta_{011}\, cos\theta} \quad (2)$$

Table 4. Crystallite size of the CFF and ACFF.

Sample	L_c (nm)	L_a (nm)
CFF	4.52	12.88
ACFF	4.44	11.71

It can be noticed a small change in L_a and L_c after the activation process. This can be explained by the formation of pores on the CFF surface after the activation process. Although the changes in L_a and L_c are not considerable, there is a significant increase in the crystallite size (Table 4).

SCANNING ELECTRON MICROSCOPY ANALYSES

The SEM images for the CFF and ACFF samples are presented in Fig. 7. From the SEM images obtained from the magnification of 1,000X, it is possible to observe the production of samples consisting of fibers of about 10 – 15μm in diameter. The SEM images also revealed the presence of smooth fibers, without

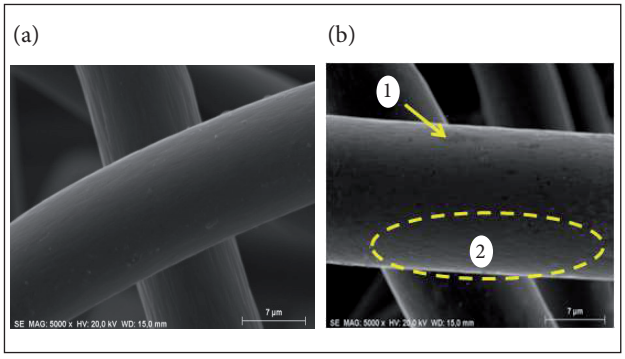

Figure 7. (a) CFF and (b) ACFF SEM images (1: Dark zones; 2: Groove region).

damages, grooves and holes. The visualization of the fiber surface with more details was possible through SEM images obtained from magnification of 5,000X. Based on these images, a smooth, clean and damage-free surface can be visualized for the CFF sample. On the other hand, the ACFF sample presents a surface containing dark zones and grooves. Pores with nano-dimension are not identified by SEM in Fig. 7. However, the presence of pores is confirmed according with Fig. 2. This morphological difference related to surface damages may be associated with the activation process. In fact, these types of damages were expected.

CONCLUSION

Activated carbon fibers produced from PAN fibers textile were successfully achieved. These studies had an important contribution regarding the understanding of the activation process on the CFF samples. The activation process plays an important role for the production of fibers with high surface and pore distribution, which are determinant to increase the exposed area. These characteristics were revealed through nitrogen adsorption isotherm analysis. XPS analysis reported the decrease in the heteroatoms quantity present in the sample, causing defects on the surface. The defects were observed by Raman spectroscopy analysis. The presence of surface imperfections was revealed through SEM images. The X-ray diffractograms showed the CFF sample had higher crystallites when compared to the ACFF one. This decrease in the crystallite size may be associated with the surface tension resulting from the activation process. Besides, the release of heteroatoms is responsible by the creation of defect, causing damage on the surface.

ACKNOWLEDGEMENTS

The authors would like to thank Fundação de Amparo à Pesquisa do Estado de São Paulo (FAPESP), Coordenação de Aperfeiçoamento de Pessoal de Nível Superior (CAPES) and Conselho Nacional de Desenvolvimento Científico e Tecnológico (CNPq) for financial support.

AUTHOR'S CONTRIBUTION

Conceptualization, Amaral Junior MA, Marcuzzo JS, and Baldan MR; Characterization, Amaral Junior MA,Marcuzzo JS, Baldan MR, and Gonçalves ES; Materials Production, Marcuzzo JS and Baldan MR; Methodology, Amaral Junior MA, Matsushima JT, Gonçalves ES, and Rezende MC; Writing – Original Draft, Amaral Junior MA and Baldan MR; Writing – Review & Editing, Amaral Junior MA, Baldan MR, and Rezende MC; Funding Acquisition, Baldan MR; Resources, Baldan MR and Marcuzzo JS; Supervision, Amaral Junior MA, Rezende MC, and Baldan MR.

REFERENCES

Beyssac O, Goffé B, Petitet JP, Froigneux E, Moreau M, Rouzaud JN (2003) On the characterization of disordered and heterogeneous carbonaceous materials by Raman spectroscopy. Spectrochimica Acta Part A: Molecular and Biomolecular Spectroscopy 59(10):2267-2276. doi: 10.1016/S1386-1425(03)00070-2

Carrott PJM, Nabais JMV, Carrott MR, Pajares JA (2001). Preparation of activated carbon fibres from acrylic textile fibres. Carbon 39(10):1543-1555. doi: 10.1016/S0008-6223(00)00271-2

Chung DDL (2004) Review electrical applications of carbon materials. J Mater Sci 39:2645-2661. doi: 10.1023/B:JMSC.0000021439.18202.ea

Cuña A, Tancredi N, Bussi J, Deiana AC, Sardella MF, Barranco V, Rojo JME (2014) Grandis as a biocarbons precursos for supercapacitor electrode application. Wast and Biomass Valor 5(1):305-313.

Hu C, Sedghi S, Silvestre-Albero A, Andersson GG, Sharma A, Pendleton P, Biggs MJ (2015) Raman spectroscopy study of the transformation of the carbonaceous skeleton of a polymer-based nanoporous carbon along the thermal annealing pathway. Carbon 85:147-158. doi: 10.1016/j.carbon.2014.12.098

Kim YK, Park H (2011) Light-harvesting multi-walled carbon nanotubes and CdS hybrids: application to photocatalytic hydrogen production from water. Energy & Environmental Science 4(3):685-694. doi: 10.1039/C0EE00330A

Lobo AO, Martin AA, Antunes EF, Trava-Airoldi VJ, Corat EJ (2005) Caracterização de materiais carbonosos por espectroscopia Raman. Revista Brasileira de Aplicações de Vácuo 24(2):98-103. doi: 10.17563/rbav.v24i2.99

Ma X, Yuan C, Liu X. (2013) Mechanical, microstructure and surface characterizations of carbon fibers prepared from cellulose after liquefying and curing. Materials 7(1):75-84. doi: 10.3390/ma7010075

Mallet-Ladeira P, Puech P, Toulouse C, Cazayous M, Ratel-Ramond N, Weisbecker P, Monthioux M (2014). A Raman study to obtain crystallite size of carbon materials: a better alternative to the Tuinstra-Koenig Law. Carbon 80:629-639.

Marcuzzo JS, Otani C, Polidoro HA, Otani S (2012) Influence of thermal treatment on porosity formation on carbon fiber from textile PAN. Mater Res 16(1):136-144.

Marsh H, Reinoso FR (2006) Activated carbon. Amsterdam: Elsevier. Chapter 4, Characterization of activated carbon; p. 143-242.

Matthews MJ, Pimenta MA, Dresselhaus G, Dresselhaus MS, Endo M. (1999) Origin of dispersive effects of the Raman D band in carbon materials. Phys Rev B 59(10):R6585. doi: 10.1103/PhysRevB.59.R6585

Nabais JV, Carrott PJM, Carrott MR (2005) From commercial textile fibres to activated carbon fibres: chemical transformations. Mater Chem Phys 93(1):100-108. doi: 10.1016/j.matchemphys.2005.02.031

Pierozynski B (2012) Electrodeposition of nickel onto 12K carbon fibre tow in a continuous manner. Croat Chem Acta 85(1):1-8. doi: 10.5562/cca1743

Sadezky A, Muckenhuber H, Grothe H, Niessner R, Pöschl U (2005) Raman microspectroscopy of soot and related carbonaceous materials: spectral analysis and structural information. Carbon 43(8):1731-1742. doi: 10.1016/j.carbon.2005.02.018

Suzuki M (1994) Activated carbon fiber: fundamentals and applications. Carbon 32(4):577-586. doi: 10.1016/0008-6223(94)90075-2

Thomsen C, Reich, S, Maultzsch J (2004) Resonant Raman spectroscopy of nanotubes. Philosophical Transactions of the Royal Society of London A: Mathematical, Physical and Engineering Sciences 362(1824):2337-2359. doi: 10.1098/rsta.2004.1444

Tuinstra F, Koenig, JL (1970). Raman spectrum of graphite. J Chem Phys 53(3):1126-1130. doi: 10.1063/1.1674108

Warren BE (1969) X-ray diffraction. North Chelmsford: Courier Corporation.

Yoon SH, Lim S, Song Y, Ota Y, Qiao W, Tanaka A, Mochida I (2004) KOH activation of carbon nanofibers. Carbon 42(8):1723-1729. doi: 10.1016/j.carbon.2004.03.006